

Characterization of microrod arrays by image analysis

Reinald Hillebrand,^{1,a)} Silko Grimm,¹ Reiner Giesa,² Hans-Werner Schmidt,² Klaus Mathwig,¹ Ulrich Gösele,¹ and Martin Steinhart¹

¹Max Planck Institute of Microstructure Physics, Weinberg 2, D-06120 Halle, Germany

²Macromolecular Chemistry I and Bayreuth Institute for Macromolecular Research (BIMF), University of Bayreuth, D-95440 Bayreuth, Germany

(Received 9 February 2009; accepted 31 March 2009; published online 22 April 2009)

The uniformity of the properties of array elements was evaluated by statistical analysis of microscopic images of array structures, assuming that the brightness of the array elements correlates quantitatively or qualitatively with a microscopically probed quantity. Derivatives and autocorrelation functions of cumulative frequency distributions of the object brightnesses were used to quantify variations in object properties throughout arrays. Thus, different specimens, the same specimen at different stages of its fabrication or use, and different imaging conditions can be compared systematically. As an example, we analyzed scanning electron micrographs of microrod arrays and calculated the percentage of broken microrods. © 2009 American Institute of Physics. [DOI: 10.1063/1.3122141]

Various microscopic techniques have been used in materials science to investigate array structures. In digital grayscale micrographs, information is encoded by the brightness or the shade of gray of the pixels they consist of. The brightness of a pixel is expressed in terms of the pixel intensity I , and array elements represented by contiguous pixels with similar I values can be identified by thresholding. In a previous work, we introduced methodologies enabling statistical grain analysis.¹ However, only quantitative statistical analysis of the properties of the individual array elements allows assessing quality, performance, and usability of the arrays they constitute. Here, we show that the classification of array elements according to their pixel intensities by successive thresholding steps yields cumulative frequency distributions (CFDs) of their brightnesses. If I quantitatively correlates with the probed physical quantity, CFDs of the properties of the array elements can thus be derived. However, as discussed below, even if only a qualitative correlation is evident, arrays can be evaluated and ranked according to their uniformity using the autocorrelation of the CFDs as a quantitative measure.

We selected arrays of aligned polyacrylate microrods as model systems that can be considered as representative examples of array configurations² used as bioinspired adhesive structures,³ surfaces with tailored wettability,⁴ substrates for tissue engineering, and drug delivery systems.⁵ Their preparation involved photocrosslinking of prepolymers (Laromer®) inside macroporous silicon templates (pore diameter of 1 μm ; pore depth of 10 μm ; lattice type: square lattice; lattice constant of 2 μm)⁶ and subsequent mechanical extraction.^{7,8} Intact microrods have convex hemispherical tips, which are replicas of the pore bottoms of the macroporous silicon templates, whereas microrods broken during their release are characterized by either smooth or slightly concave fracture faces. Digital grayscale images with a size of 1280×1000 pixels and an image depth of 8 bits ranging from $I=0$ (black) to $I=255$ (white) were obtained on

a JEOL 7500F scanning electron microscope (SEM) using a lower secondary electron imaging detector (Everhart–Thornley type). The angle between incident electron beam and the normal to the surface of the sample holder was 30° . We selected three exemplary micrographs for detailed analysis using the program ImageJ.⁹ Sample A [Fig. 1(a)] is uniformly illuminated and consists of intact microrods [Fig. 1(a), inset]; sample B [Fig. 1(b)] is uniformly illuminated but contains a significant portion of fractured microrods [Fig. 1(b), inset], and; sample C [Fig. 1(c)] consist of intact microrods [Fig. 1(c), inset] but exhibits long-range contrast variations caused by specimen charging effects. Under the conditions applied here, the convex hemispherical tips of intact microrods appear brighter than the fracture faces of the broken ones.

Histograms of digital images represent the distribution of pixels with certain pixel intensities. We performed consecutive thresholding steps by shifting the lower threshold I_T in the histograms of the SEM images of samples A, B, and C from 0 toward 255 with an increment of $\Delta I_T=10$. For example, in Fig. 2 the I_T value was set to 120. Areas with $I \geq 120$ are white; areas with $I < 120$ are black. Classes were obtained by counting all separate objects, here the tips of the microrods with $I \geq I_T$, while discarding all darker entities. N denotes the number of objects belonging to a class. The number of classes containing more than one object, which were considered for the compilation of $N(I_T)$ profiles [Fig. 3(a)], is denoted by M and depends on the overall contrast in the analyzed image. The $N(I_T)$ profiles are CFDs of the brightnesses of the identified objects, on which, however, contrast saturation effects may superimpose. Their slopes, expressed by the difference quotients $\Delta N/\Delta I_T$, are plotted in Fig. 3(b) as a function of I_T . Only large contiguous areas are recognized at low I_T values, into which the tips of the microrods are merged. As I_T is shifted to higher values, the dark background between the brighter tips of the microrods is discarded. Hence, the tips start to appear as separate objects, and $N(I_T)$ steeply increases ($\Delta N/\Delta I_T \gg 0$) up to a global maximum N_{max} corresponding to the total number of imaged microrods ($\Delta N/\Delta I_T=0$). The $N(I_T)$ profile of sample A ex-

^{a)}Electronic mail: hi@mpi-halle.mpg.de. Tel.: 049 + 345 + 5582 911. FAX: 049 + 345 + 5511 223.

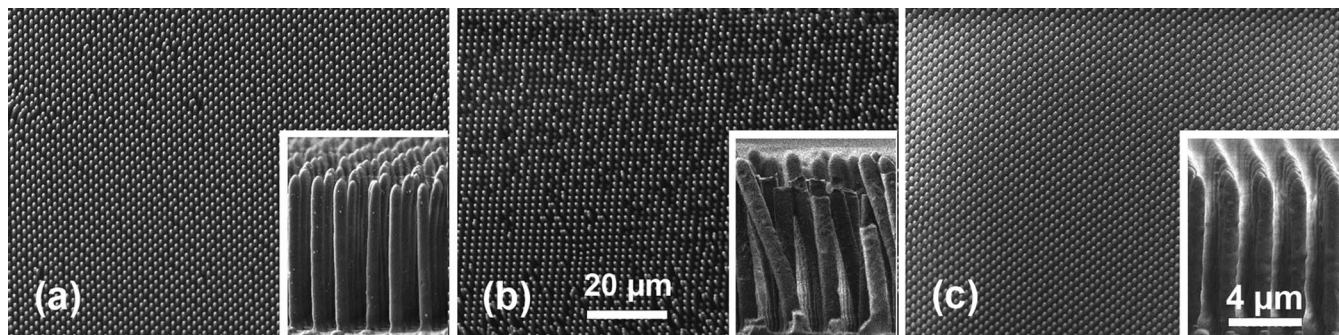


FIG. 1. SEM top views of polyacrylate microrod arrays released from macroporous silicon templates taken in the lower secondary electron detection mode at various accelerating voltages U . (a) Sample A: polyacrylate PO 77F, $U=2$ keV. (b) Sample B: polyacrylate PO 77F-MX, $U=7$ keV. (c) Sample C: polyacrylate LR 9007, $U=2$ keV. The insets show the corresponding side-views.

hibits a pronounced plateau in the interval $I_T \in [100, 180]$, within which the number of recognized microrods remains constant ($\Delta N/\Delta I_T \approx 0$) and corresponds to N_{\max} . The steep decrease in $N(I_T)$ for $I_T > 180$ ($\Delta N/\Delta I_T \ll 0$) suggests that the tips of the microrods are highly uniform in brightness ($I \approx 180$) and, therefore, nearly exclusively convex throughout the imaged area. Thus, the portion of fractured microrods in sample A is negligible. Sample B contains both intact microrods with bright convex tips and broken ones. N_{\max} amounts to 2704 and is reached at $I_T \approx 90$ ($\Delta N/\Delta I_T \approx 0$). In the interval $I_T \in [90, 150]$ marked by arrows in Fig. 3(b), $N(I_T)$ continuously decreases because fractured microrods with $I < I_T$ are no longer recognized and merge into the background. Directly above $I_T = 90$ a pronounced drop in $N(I_T)$ is evident ($\Delta N/\Delta I_T < 0$), whereas $\Delta N/\Delta I_T$ approaches zero at $I_T = 140$. Even a small plateau is evident between $I_T = 140$ and $I_T = 150$ ($\Delta N/\Delta I_T \approx 0$). At $I_T \approx 150$ only the intact microrods having convex tips are recognized that eventually disappear within a narrow I_T interval ($\Delta N/\Delta I_T \ll 0$; I_T exceeds I value of the intact microrods). The portion of fractured microrods is equivalent to the relative loss $-100(\Delta N/\Delta I_T)/N_{\max}$ in an interval defined by the I_T value of N_{\max} and that above which intact microrods with convex tips merge into the background. Summing up the relative loss in microrods upon successive increase in I_T by $\Delta I_T = 10$ in the interval $I_T \in [100, 150]$ reveals that in sample B 31.2% of the microrods were fractured [Fig. 3(c)]. In the SEM image of sample C, the I_T value belonging to N_{\max} is 130. Large contiguous areas counted as single entities are seen in the outer left and right parts, while the tips of the microrods in the center start to merge into the background for $I_T > 130$. Hence, the $N(I_T)$ profile of sample C exhibits only a narrow maximum at $I_T = 130$, and $\Delta N/\Delta I_T$ decreases nearly linearly as I_T increases [Fig. 3(b)]. Contrast saturation effects thus superimpose on changes in $N(I_T)$ related to the topography of sample C over the entire I_T range.

To directly compare the global uniformity of the image properties, including sample topography and illumination of

the image field, in micrographs displaying different numbers of array elements, we normalized the $N(I_T)$ profiles to unity and calculated their autocorrelation functions (ACFs) according to¹⁰

$$AC_j \approx \frac{1}{M-j} \sum_{i=1}^{M-j} N(I_T)_i \times N(I_T)_{i+j}.$$

AC_j is the correlation between a $N(I_T)$ profile and its duplicate shifted by j steps, whereas $i=1, 2, \dots, M$ and $j=1, 2, \dots, M-1$ are integers. The ACFs in Fig. 3(d), which were normalized to M , are characterized by monotonic decay of AC_j that evidences the absence of random or periodic patterns. The self-similarity of the $N(I_T)$ profiles is quantified

by the sums $S = \sum_{k=1}^j AC_k$ representing the areas under the corresponding ACFs as well as by the widths at half maximum (WHM) of the ACFs. High S values stand for high overall self-similarity. High WHM values occur if many classes are highly populated and indicate dominance of local specimen properties over contrast saturation. The S and WHM values indeed capture the characteristic features of samples A–C (Table I). The large number of fractured microrods in sample B and the long-range brightness variations in sample C result in S values significantly smaller than that of sample A. Samples A and B have large WHM values reflecting their uniform illumination, whereas that of sample C is smaller.

In conclusion, we have evaluated the uniformity of array elements by statistical analysis of digital microscopic images of array structures. CFDs of the brightnesses of the array elements were obtained by successive thresholding steps, recognition of the individual objects and their classification according to their pixel intensities. As shown above, a qualitative correlation between brightness and object properties is sufficient for the evaluation of assemblies. As an example in case, we analyzed SEM images of arrays of aligned polymer microrods, taking advantage of differences in brightness between intact and fractured microrods related to their tip



FIG. 2. Thresholded upper halves of the SEM images shown in Fig. 1 ($I_T=120$). (a) Sample A, (b) sample B, and (c) sample C.

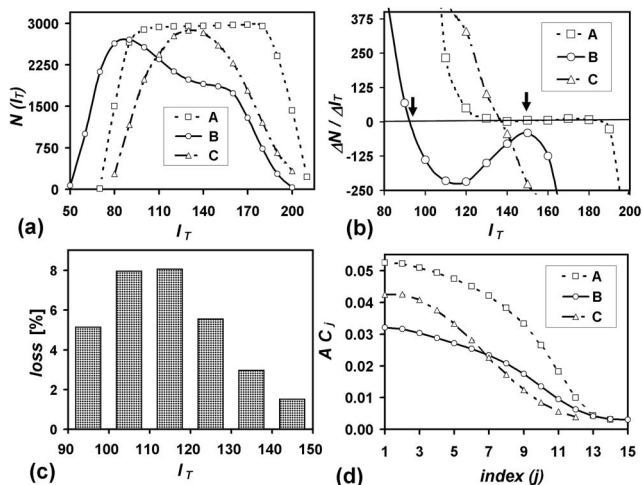


FIG. 3. Analysis of the SEM images of samples A–C. (a) Number of recognized microrods N as a function of the lower threshold I_T . (b) Slope $\Delta N / \Delta I_T$ of the $N(I_T)$ profiles shown in (a). (c) Fractured microrods in sample B merging into the background in the I_T interval marked by arrows in (b). (d) Autocorrelation $AC(j)$ normalized to the number of considered classes M of the $N(I_T)$ profiles of samples A–C that were in turn normalized to unity.

shapes. Moreover, we calculated the percentage of broken microrods. The imaged arrays were rated according to their global uniformity based on the areas and widths at half maximum of the ACFs of the CFDs. If the brightness quantitatively correlates with a probed physical quantity, CFDs of the physical properties of the array elements are accessible. Different arrays, the same array at different stages of its fabrication or use, as well as different contrast formation mecha-

TABLE I. Parameters S and WHM quantifying the uniformity of samples A–C.

Sample	A	B	C
S	0.43	0.23	0.26
WHM	10	9	7

nisms or imaging conditions can be compared systematically.

The authors thank the German Research Foundation for financial support (Materials World Network, Contract No. STE 1127/5 and SFB 481, Project A6), BASF SE for the donation of Laromer® resins, W. Erfurth for critical discussions, and K. Sklarek as well as M. Gietl for technical support.

¹R. Hillebrand, F. Müller, K. Schwirn, W. Lee, and M. Steinhart, *ACS Nano* **2**, 913 (2008).

²A. del Campo and E. Arzt, *Chem. Rev. (Washington, D.C.)* **108**, 911 (2008).

³H. Lee, B. P. Lee, and P. B. Messersmith, *Nature (London)* **448**, 338 (2007).

⁴X. Feng and L. Jiang, *Adv. Mater. (Weinheim, Ger.)* **18**, 3063 (2006).

⁵S. L. Tao and T. A. Desai, *Nano Lett.* **7**, 1463 (2007).

⁶V. Lehmann, *J. Electrochem. Soc.* **140**, 2836 (1993).

⁷S. Grimm, K. Schwirn, K. P. Göring, H. Knoll, P. T. Miclea, A. Greiner, J. Wendorff, R. B. Wehrspohn, U. Gösele, and M. Steinhart, *Small* **3**, 993 (2007).

⁸S. Grimm, R. Giesa, K. Sklarek, A. Langner, U. Gösele, H.-W. Schmidt, and M. Steinhart, *Nano Lett.* **8**, 1954 (2008).

⁹W. Rasband, ImageJ, release 1.36b, NIH, USA, 2006 (<http://rsb.info.nih.gov/ij/>).

¹⁰*Numerical Recipes in FORTRAN*, 2nd ed., edited by W. H. Press, S. A. Teukolsky, W. T. Vetterling, and B. P. Flannery (Cambridge University Press, Cambridge, 1992), Chap. 13.